INSTITUTE OF PHYSICS PUBLISHING JOURNAL OF PHYSICS A: MATHEMATICAL AND GENERAL

J. Phys. A: Math. Gen. **39** (2006) 1163–1181 doi:10.1088/0305-4470/39/5/010

First-principles quantum dynamics in interacting Bose gases: I. The positive P representation

P Deuar and P D Drummond[1]

Australian Centre for Quantum Atom Optics, The University of Queensland, Brisbane, Australia

E-mail: deuar@physics.uq.edu.au and drummond@physics.uq.edu.au

Received 21 June 2005, in final form 28 November 2005
Published 18 January 2006
Online at stacks.iop.org/JPhysA/39/1163

Abstract

The performance of the positive P phase-space representation for exact many-body quantum dynamics is investigated. Gases of interacting bosons are considered, where the full quantum equations to simulate are of a Gross–Pitaevskii form with added Gaussian noise. This method gives tractable simulations of many-body systems because the number of variables scales linearly with the spatial lattice size. An expression for the useful simulation time is obtained, and checked in numerical simulations. The dynamics of first-, second- and third-order spatial correlations are calculated for a uniform interacting 1D Bose gas subjected to a change in scattering length. Propagation of correlations is seen. A comparison is made with other recent methods. The positive P method is particularly well suited to open systems as no conservation laws are hard-wired into the calculation. It also differs from most other recent approaches in that there is no truncation of any kind.

PACS numbers: 03.75.Kk, 05.10.Gg, 03.65.Yz, 02.50.Ey

1. Introduction

Simulation of exact many-body quantum dynamics is a highly non-trivial task even in the simplest models. However, such a capability is highly desirable for studies of the quantum behaviour of mesoscopic systems. First-principles methods are particularly useful when there are several length, time or energy scales of similar size, which makes simplifying approximations inaccurate. It is well known, however, that a calculation using an orthogonal basis is intractable because the size of the Hilbert space needed to accurately describe the state grows exponentially with the number of subsystems. Perturbation theory is often not useful either, owing to questions of convergence. Other commonly used techniques—such

[1] www.physics.uq.edu.au/BEC.

as the mean-field approximation—rely on factorizations of operator products, with unknown regimes of validity.

A promising approach is to simulate stochastic equations derived from phase-space distribution methods such as the positive P [1, 2] and gauge P [3] representations, or representations based on other separable basis sets. In such methods the quantum state is written as a probability distribution of off-diagonal system configurations, which are separable between local subsystems. For the case of the positive P representation, these subsystems are the spatial lattice points. The number of variables needed to specify a single configuration grows only *linearly* with the system size because they are separable. Correlations between subsystems are contained in the details of the distribution, which is stochastically sampled. This very mild growth of the number of required variables is the reason that such methods lead to tractable many-body simulations. Recent work has shown that any model with two-body interactions can be expressed by such a distribution of separable system configurations [4].

In this paper we develop reliable ways of estimating the feasible simulation time, which is limited in practice by the growth of the statistical error. This allows an assessment of simulation parameters before a potentially lengthy calculation is started. We apply our method to single and coupled anharmonic oscillators, and compare analytic and numerical results for the simulation time. We also investigate the quantum dynamics of a one-dimensional interacting Bose gas. This calculation shows a unique and interesting behaviour under conditions of a sudden switch in the interaction strength. We observe correlation waves in which an otherwise homogeneous quantum gas develops wave-like structures found only in the relative coordinates.

This is a particularly timely issue in view of recent developments in fibre optics and ultra-cold atomic Bose gases. It is now possible to experimentally investigate large numbers of interacting bosons, under conditions where quantum coherence plays an important role. As an example, quadrature squeezing in quantum solitons was predicted using these techniques, and observed experimentally. Ultra-cold atomic Bose gas dynamics has been observed in a number of geometries. In these experiments, it is possible to modify external potentials in order to drive the quantum gas into a state very far from either the ground state or any thermal equilibrium state. More recently, experiments have demonstrated the possibility of dynamically varying the inter-particle potential.

The main body of the paper is organized as follows: first the positive P method is summarized in section 2, and briefly compared to other approaches in section 3. Subsequently in sections 4 and 6, the estimates of useful integration times are obtained and their implications are considered. These estimates are verified by numerical simulations of single-mode and multi-mode systems, in sections 5 and 7, respectively. As an example, in the latter section, the dynamics of spatial correlation functions in a 1D uniform gas are investigated. We consider the effects of an experiment in which the inter-particle potential is suddenly changed. This is potentially observable using the technique of a Feshbach resonance in an external magnetic field.

In a subsequent paper [5], we consider the more sophisticated stochastic gauge method for these types of simulations.

2. Model

2.1. The lattice model

We consider a dilute interacting Bose gas. In the continuum, the second-quantized Hamiltonian with kinetic terms, two-body interactions with inter-particle potential $U(\mathbf{r})$ and external

potential $V_{\rm ext}(\mathbf{x})$ is

$$\widehat{H} = \int \left[\frac{\hbar^2}{2m} \nabla \widehat{\Psi}^\dagger(\mathbf{x}) \nabla \widehat{\Psi}(\mathbf{x}) + V_{\rm ext}(\mathbf{x}) \widehat{\Psi}^\dagger(\mathbf{x}) \widehat{\Psi}(\mathbf{x}) + \frac{U(\mathbf{x}-\mathbf{y})}{2} \widehat{\Psi}^\dagger(\mathbf{x}) \widehat{\Psi}^\dagger(\mathbf{y}) \widehat{\Psi}(\mathbf{x}) \widehat{\Psi}(\mathbf{y}) \right] \mathrm{d}^3\mathbf{x}. \tag{1}$$

Here $\widehat{\Psi}(\mathbf{x})$ is a boson-field operator at $\mathbf{x}$ and m is the boson mass.

In practice, (1) is replaced by a lattice Hamiltonian, which contains all the essential features provided the lattice spacing is sufficiently small. For a rarefied gas of the kind occurring in contemporary BEC experiments, s-wave scattering dominates [6], and the s-wave scattering length a_s is much smaller than all other relevant length scales. If the lattice spacing is also much larger than a_s, then the two-body scattering is well described by an interaction local at each lattice point.

Let us label the spatial dimensions by $d = 1, \ldots, D$ and lattice points by the vectors $\mathbf{n} = (n_1, \ldots, n_D)$. For lattice spacings Δx_d, the spatial coordinates of the lattice points are $\mathbf{x_n} = (n_1 \Delta x_1, \ldots, n_D \Delta x_D)$. The volume per lattice point is $\Delta V = \prod_d \Delta x_d$. We also define the lattice annihilation operators $\widehat{a}_\mathbf{n} \approx \sqrt{\Delta V}\widehat{\Psi}(\mathbf{x_n})$, which obey the usual boson commutation relations of $\left[\widehat{a}_\mathbf{n}, \widehat{a}_\mathbf{m}^\dagger\right] = \delta_\mathbf{nm}$. With these definitions, one obtains

$$\widehat{H} = \hbar \left[\sum_{\mathbf{nm}} \omega_\mathbf{nm} \widehat{a}_\mathbf{n}^\dagger \widehat{a}_\mathbf{m} + \frac{1}{2} \sum_\mathbf{n} \kappa \widehat{a}^{\dagger 2} \widehat{a}^2 \right]. \tag{2}$$

In this normally ordered Hamiltonian, the frequency terms $\omega_\mathbf{nm} = \omega_\mathbf{mn}^*$ come from the kinetic energy and external potential. They produce a local particle-number-dependent energy, and linear coupling to other sites, the latter arising only from the kinetic processes. The nonlinearity due to local particle–particle interactions is of strength

$$\kappa = \frac{g}{\hbar \Delta V}, \tag{3}$$

with the standard coupling value [6] being $g = g_{3\rm D} = 4\pi a_s \hbar^2/m$ in 3D, and $g = g_{3\rm D}/\sigma$ in 2D and 1D, where σ is the effective thickness or cross-section of the collapsed dimensions.

When interaction with the environment is Markovian (i.e. no feedback), the evolution of the density matrix $\widehat{\rho}$ can be written as a master equation in Linblad form

$$\frac{\partial \widehat{\rho}}{\partial t} = \frac{1}{\mathrm{i}\hbar}[\widehat{H}, \widehat{\rho}] + \frac{1}{2} \sum_j \left[2\widehat{L}_j \widehat{\rho} \widehat{L}_j^\dagger - \widehat{L}_j^\dagger \widehat{L}_j \widehat{\rho} - \widehat{\rho} \widehat{L}_j^\dagger \widehat{L}_j \right]. \tag{4}$$

For example, single-particle losses at rate $\gamma_\mathbf{n}$ (at $\mathbf{x_n}$) to a $T = 0$ heat bath are described by $\widehat{L}_\mathbf{n} = \widehat{a}_\mathbf{n} \sqrt{\gamma_\mathbf{n}}$.

2.2. Positive P representation

The positive P representation was developed in [1, 2]. Here we summarize the issues relevant to the dynamics of model (1), and present the stochastic equations to simulate.

For a lattice with M points, the density matrix is expanded as

$$\widehat{\rho} = \int P_+(\boldsymbol{\alpha}, \boldsymbol{\beta}) \widehat{\Lambda}(\boldsymbol{\alpha}, \boldsymbol{\beta}) \, \mathrm{d}^{2M}\boldsymbol{\alpha} \, \mathrm{d}^{2M}\boldsymbol{\beta}, \tag{5}$$

where $\widehat{\Lambda}$ is an off-diagonal operator kernel, separable between the M lattice point subsystems. We use a coherent-state basis so that

$$\widehat{\Lambda}(\boldsymbol{\alpha}, \boldsymbol{\beta}) = \|\boldsymbol{\alpha}\rangle\langle\boldsymbol{\beta}^*\| \exp[-\boldsymbol{\alpha} \cdot \boldsymbol{\beta}], \tag{6}$$

in terms of Bargmann coherent states with complex amplitudes $\boldsymbol{\alpha} = (\ldots, \alpha_{\mathbf{n}}, \ldots)$:

$$\|\boldsymbol{\alpha}\rangle = \otimes_{\mathbf{n}} \exp\left[\alpha_{\mathbf{n}} \widehat{a}_{\mathbf{n}}^{\dagger}\right]|0\rangle. \tag{7}$$

The gauge P representation mentioned previously [3] includes an extra global weight in the kernel, which allows useful modifications of the final stochastic equations [7, 3, 5, 8].

It has been shown that all density matrices can be represented by a positive real P_+ [2]. Expansion (5) then becomes a probability distribution of $\widehat{\Lambda}$, or equivalently of the variables $\boldsymbol{\alpha}, \boldsymbol{\beta}$. A constructive expression for $P_+(\widehat{\rho})$ is given by expression (3.7) in [2], although more compact distributions may exist. In particular, a coherent state $|\boldsymbol{\alpha}_0\rangle$ will simply have

$$P_+ = \delta^{2M}(\boldsymbol{\alpha} - \boldsymbol{\alpha}_0)\delta^{2M}(\boldsymbol{\beta} - \boldsymbol{\alpha}_0^*). \tag{8}$$

Using the identities

$$\widehat{a}_{\mathbf{n}}\widehat{\Lambda} = \alpha_{\mathbf{n}}\widehat{\Lambda}, \tag{9a}$$

$$\widehat{a}_{\mathbf{n}}^{\dagger}\widehat{\Lambda} = \left[\beta_{\mathbf{n}} + \frac{\partial}{\partial \alpha_{\mathbf{n}}}\right]\widehat{\Lambda}, \tag{9b}$$

the master equation (4) in $\widehat{\rho}$ can be shown to be equivalent to a Fokker–Planck equation in P_+, and then to stochastic equations in $\alpha_{\mathbf{n}}$ and $\boldsymbol{\beta}_{\mathbf{n}}$. The standard method is described in [9]. The correspondence is in the sense that appropriate stochastic averages of $\alpha_{\mathbf{n}}$ and $\beta_{\mathbf{n}}$ correspond to quantum expectation values in the limit when the number of trajectories $\mathcal{S} \to \infty$. In particular one finds that [7]

$$\left\langle \prod_{jk} \widehat{a}_{\mathbf{n}_j}^{\dagger} \widehat{a}_{\mathbf{n}_k} \right\rangle = \lim_{\mathcal{S}\to\infty} \left\langle \prod_{jk} \beta_{\mathbf{n}_j} \alpha_{\mathbf{n}_k} + \prod_{jk} \beta_{\mathbf{n}_k}^* \alpha_{\mathbf{n}_j}^* \right\rangle_{\mathrm{s}}. \tag{10}$$

Any observable can be written as a linear combination of terms (10). We will use the notation $\langle\cdot\rangle_{\mathrm{s}}$ to distinguish stochastic averages of random variables from quantum expectations $\langle\cdot\rangle$.

The resulting $2M$ Ito complex stochastic equations are found using methods described in [2, 9]. For model (2) obeying the master equation (4) with coupling to a zero temperature heat bath, they are of the Gross–Pitaevskii (GP) form, plus noise:

$$\begin{aligned} \mathrm{d}\alpha_{\mathbf{n}} &= \left[-\mathrm{i}\sum_{\mathbf{m}} \omega_{\mathbf{nm}}\alpha_{\mathbf{m}} - \mathrm{i}\kappa n_{\mathbf{n}}\alpha_{\mathbf{n}} - \gamma_{\mathbf{n}}\alpha_{\mathbf{n}}/2\right]\mathrm{d}t + \sum_k B_{\mathbf{n}k}^{(\alpha)}\,\mathrm{d}W_k, \\ \mathrm{d}\beta_{\mathbf{n}} &= \left[\mathrm{i}\sum_{\mathbf{m}} \omega_{\mathbf{nm}}^*\beta_{\mathbf{m}} + \mathrm{i}\kappa n_{\mathbf{n}}\beta_{\mathbf{n}} - \gamma_{\mathbf{n}}\beta_{\mathbf{n}}/2\right]\mathrm{d}t + \sum_k B_{\mathbf{n}k}^{(\beta)}\,\mathrm{d}W_k. \end{aligned} \tag{11}$$

Here, $n_{\mathbf{n}} = \alpha_{\mathbf{n}}\beta_{\mathbf{n}}$, and there are $M' \geqslant 2M$ labels k to sum over. The $\mathrm{d}W_k$ are independent Wiener increments $\langle \mathrm{d}W_j(t)\,\mathrm{d}W_k(s)\rangle_{\mathrm{s}} = \delta_{jk}\delta(t-s)\,\mathrm{d}t^2$. In practice, these can be realized at each time step Δt by independent real Gaussian noises of mean zero and variance Δt. The elements of the $M \times M'$ *noise matrices* B must satisfy

$$\begin{aligned} \sum_k B_{\mathbf{n}k}^{(\alpha)} B_{\mathbf{m}k}^{(\alpha)} &= -\mathrm{i}\kappa\alpha_{\mathbf{n}}^2\delta_{\mathbf{nm}}, \\ \sum_k B_{\mathbf{n}k}^{(\beta)} B_{\mathbf{m}k}^{(\beta)} &= \mathrm{i}\kappa\beta_{\mathbf{n}}^2\delta_{\mathbf{nm}}, \\ \sum_k B_{\mathbf{n}k}^{(\alpha)} B_{\mathbf{m}k}^{(\beta)} &= 0. \end{aligned} \tag{12}$$

Table 1. Some general features of several methods for simulation of many-body dynamics. M is the number of lattice points, and N is the number of particles. d is the Hilbert space dimension of the subsystem at each lattice point, D is the dimension of each corresponding ancillary state after possible truncation of entanglement in the DMRG-based methods.

	Stochastic gauge positive P	Stochastic wavefunction	DMRG-based methods
Subsystems	Lattice points	Particles	d-Level systems
Stochastic	Yes	Yes	No
Hard-wired conservation laws	None	Particle number	d-Level systems
Open systems	Yes	No	Yes
Truncation	None	None	Entanglement
Tractable coupling	Wide variety	Wide variety	Short-range or 1D
Memory requirements	$\propto M$	$\propto M$	$\propto MdD$
Hilbert space dimension	∞^M	M^N	d^M
References	[1, 2, 7, 3, 13, 8]	[14, 15]	[16–18]

These do not actually specify the elements of B completely. The usefulness of these degrees of freedom is considered in detail in [3, 5, 8], but here we will just use the simplest choices

$$B^{(\alpha)}_{\mathbf{n}_j k} = \mathrm{i}\sqrt{\mathrm{i}\kappa}\alpha_{\mathbf{n}_j}\delta_{j,k}, \qquad B^{(\beta)}_{\mathbf{n}_j k} = \sqrt{\mathrm{i}\kappa}\beta_{\mathbf{n}_j}\delta_{(j+M),k}, \tag{13}$$

where $k = 1, \ldots, 2M$. The indices $j = 1, \ldots, M$ label the lattice points.

The simulation strategy is (briefly) as follows:

(i) sample a trajectory according to the known initial condition $P_+(0) = P_+(\widehat{\rho}(0))$;
(ii) evolve according to the stochastic equations (11), calculating moments of interest and recording;
(iii) repeat for $\mathcal{S} \gg 1$ independent trajectories and average.

3. Comparison with other dynamical methods

Several positive P and gauge P simulations of the models of section 2.1 (or very similar) have already appeared:

- quantum optical soliton propagation in nonlinear Kerr media [10], which obeys a Hamiltonian formally very similar to (1);
- dynamics of evaporative cooling and incipient condensation of an interacting Bose gas [11, 12];
- thermal and dynamical behaviour of spatial correlations in one-dimensional interacting Bose gases [8, 13] using the stochastic gauge representation [3, 7].

Some of the other many-mode dynamics simulation methods proposed more recently include (see table 1 for a visual comparison) the following two methods.

The *stochastic wavefunction* method of Carusotto, Castin and Dalibard [14, 15] shares many common features with the gauge P method [8]. It is also based on a phase-space distribution over separable operators with a global weight, and can be regarded formally as a particular choice of gauge and basis set. In this case the separable 'subsystems' are chosen to be exactly N identical particles, rather than the M spatial lattice points of the gauge P/positive P approach. Hence, sampled variables specify an orbital occupied by these N particles, rather than the conditions at each lattice point. This explicitly imposes both a precise particle number and particle conservation on the model, and so makes the method directly applicable only to closed models where processes such as random losses, outcoupling or gain are absent.

Where both stochastic gauge and stochastic wavefunction methods can be applied, the useful simulation time is similar [5].

A different approach is entirely based on extensions of the *density matrix renormalization group* (DMRG) method [16, 17]. This method is based on the concept that an N-subsystem state is equivalent to a construction called a matrix product state (MPS) in a larger Hilbert space. This involves a further N 'ancillary' systems entangled with the original subsystems. In cases where entanglement between the original subsystems is small or short-range (such as spin chains with nearest-neighbour interactions), a good approximation to the full state can be obtained by truncating the amount of entanglement present in the MPS construction. These truncated states can be stored efficiently with a number of variables polynomial in N, due to the way the MPS states are constructed. This can lead to tractable *deterministic* calculations even with significant N. For longer-range coupling in 2D and 3D, there are indications based on the entropy of bipartite entanglement that the amount of entanglement is expected to grow too fast for tractable accurate simulations with this method [18].

While each approach has its own merits, for large and/or 2D, 3D systems the stochastic phase-space methods appear to be the most efficient, perhaps apart from special cases. There, for the price of limited precision, one can obtain an untruncated first-principles simulation whose demands on resources and time scale only linearly with size. For open systems, the methods based on lattice point subsystems (such as the positive P) can be applied in a straightforward manner, as they explicitly allow a varying particle number. In contrast, attempts to use orbital-based states as in the stochastic wavefunction lead at best to additional complication.

4. Single-mode simulation times

4.1. Exactly solvable single-mode model

The single-mode case is of special interest as it is exactly solvable, while still describing an interacting many-body quantum system. It already contains the essential features that make the distribution of trajectories broaden, thus limiting the useful simulation time.

To simplify the notation, the mode labels $\mathbf{n} = (0, \ldots, 0)$ will be omitted when referring to the single-mode system. Furthermore, we move to an interaction picture where the harmonic oscillator evolution due to the $\hbar\omega\widehat{a}^\dagger\widehat{a}$ term in the Hamiltonian is implicitly contained within the Heisenberg evolution of the operators. Then, this 'anharmonic oscillator' model has

$$\widehat{H} = \frac{\hbar\kappa}{2}\widehat{a}^{\dagger 2}\widehat{a}^2, \tag{14}$$

and the equations to simulate are

$$\mathrm{d}\alpha = \alpha[-\mathrm{i}\kappa n\,\mathrm{d}t - \gamma\,\mathrm{d}t/2 + \mathrm{i}\sqrt{\mathrm{i}\kappa}\,\mathrm{d}W_1], \qquad \mathrm{d}\beta = \beta[\mathrm{i}\kappa n\,\mathrm{d}t - \gamma\,\mathrm{d}t/2 + \sqrt{\mathrm{i}\kappa}\,\mathrm{d}W_2], \tag{15}$$

with $n = \alpha\beta$. Note that by (10), the mode occupation $\langle\widehat{a}^\dagger\widehat{a}\rangle$ is $\langle\mathrm{Re}[n]\rangle_\mathrm{s}$.

These equations can be formally solved using the rules of Ito calculus as

$$\log n(t) = \log n(0) - \gamma t + \sqrt{\mathrm{i}\kappa}[\zeta_2(t) + \mathrm{i}\zeta_1(t)], \tag{16a}$$

$$\log\alpha(t) = \log\alpha(0) + (\mathrm{i}\kappa - \gamma)t/2 + \mathrm{i}\sqrt{\mathrm{i}\kappa}\zeta_1(t) - \mathrm{i}\kappa\int_0^t n(s)\,\mathrm{d}s, \tag{16b}$$

where

$$\zeta_j(t) = \int_0^{W(t)} \mathrm{d}W \tag{16c}$$

are the Gaussian-distributed random variables of mean zero. However, they are not time independent:

$$\langle \zeta_j(t)\zeta_k(s)\rangle_{\rm s} = \delta_{jk}\,\min[t,s]. \tag{17}$$

In what follows it will be convenient to consider the evolution of an off-diagonal coherent-state kernel

$$\widehat{\Lambda}_0 = \widehat{\Lambda}(\alpha_0,\beta_0), \tag{18}$$

with complex 'particle number' $n_0 = \alpha_0\beta_0$. This is because for any general initial state, each sampled trajectory will start out as $\widehat{\Lambda}_0$ with some coherent amplitudes.

With initial condition $\widehat{\Lambda}_0$, analytic expressions for observables can be readily obtained. In particular, we will calculate the first-order time-correlation function

$$G^{(1)}(0,t) = \beta_0\langle\widehat{a}\,\rangle = \alpha_0^*\langle\widehat{a}^\dagger\rangle^*, \tag{19}$$

which contains phase coherence information. Normalizing by $\mathrm{Tr}[\widehat{\Lambda}_0]$,

$$G^{(1)}(0,t) = n_0\,{\rm e}^{-\gamma t/2}\exp\left\{\frac{n_0}{1-{\rm i}\gamma/\kappa}({\rm e}^{-{\rm i}\kappa t-\gamma t}-1)\right\}. \tag{20}$$

When the damping is negligible, n_0 real, and the number of particles is $n_0 \gg 1$, one sees that the initial phase oscillation period is

$$t_{\rm osc} = \frac{1}{\kappa}\sin^{-1}\left(\frac{2\pi}{n_0}\right) \approx \frac{2\pi}{\kappa n_0}, \tag{21}$$

and the phase coherence time, over which $|G^{(1)}(0,t)|$ decays is

$$t_{\rm coh} = \frac{1}{\kappa}\cos^{-1}\left(1-\frac{1}{2n_0}\right) \approx \frac{1}{\kappa\sqrt{n_0}}. \tag{22}$$

The first quantum revival occurs at

$$t_{\rm revival} = \frac{2\pi}{\kappa}. \tag{23}$$

4.2. Causes of growth of sampling error

From (16), $\log n(t)$ is Gaussian distributed, while $\log\alpha(t)$ is also Gaussian-like, at least at short times when the effect of the nonlinear term is negligible. The variables α and $\beta = n/\alpha$ appearing in observable calculations behave approximately as exponentials of Gaussian random variables, at least over short times. Hence, the properties of this kind of random quantity can tell us much about the behaviour of the simulation.

If ξ is a Gaussian random variable of mean zero, variance unity, let us define

$$v = v_0\,{\rm e}^{\sigma\xi} \tag{24}$$

with real positive σ. The even m moments of ξ are

$$\lim_{\mathcal{S}\to\infty}\langle\xi(t)^m\rangle_{\rm s} = \frac{m!}{2^{m/2}(m/2)!}, \tag{25}$$

while the odd m moments are zero. This can be used to obtain

$$\lim_{\mathcal{S}\to\infty}\langle v\rangle_{\rm s} = \overline{v} = v_0\exp\left(\frac{\sigma^2}{2}\right) \tag{26}$$

and

$$\lim_{\mathcal{S}\to\infty}\mathrm{var}\left[\frac{v}{\overline{v}}\right] = {\rm e}^{\sigma^2}-1, \tag{27}$$

i.e. the standard deviation of v is linear in σ for $\sigma \lesssim 1$, but grows rapidly once $\sigma \gtrsim 1$.

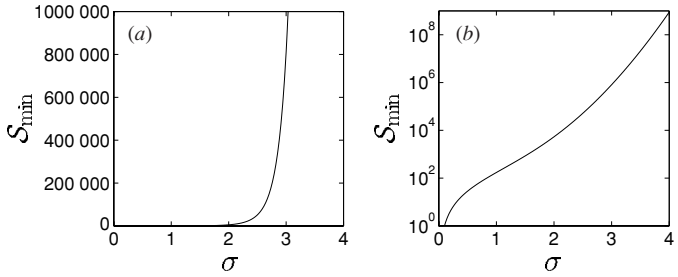

Figure 1. Number of samples $\mathcal{S}_{\min}$ required to obtain a single significant digit of precision in $\overline{v}$, the estimate of the mean of the random variable $v = e^{\sigma\xi}$.

With finite samples $\mathcal{S}$, the fluctuations of $\langle v\rangle_s$ around $\overline{v}$ are usually estimated to be

$$\Delta\overline{v} \approx \sqrt{\frac{\mathrm{var}[v]}{\mathcal{S}}} \tag{28}$$

using the central limit theorem (CLT). Hence, the number of samples needed to achieve a given relative precision is

$$\mathcal{S} \propto \mathrm{var}[v/\overline{v}]. \tag{29}$$

This is shown in figure 1. In particular, we see that simulations with reasonable numbers of trajectories $\mathcal{S} \lesssim \mathrm{O}(10^6)$ only give useful precision while

$$\sigma^2 \lesssim 10. \tag{30}$$

In actual calculations of moments, from (10) we see that common observables are estimated by averages $\langle f\rangle_s$, where f is a polynomial in α and/or n. Because the exact solutions (16) are Gaussian-like, f behaves similarly to the idealized variable v discussed above, and useful precision will be limited by

$$\mathrm{var}[\log|f|] \lesssim \mathrm{O}(10). \tag{31}$$

in analogy with (30). We have switched to O(10) rather than just 10 here, because the details of the distribution of $\log|f|$ may differ from a Gaussian at long times due to the nonlinear term $\propto \int n$ in (16).

Observables that are first order in $\widehat{a}, \widehat{a}^\dagger$ (such as $G^{(1)}(0,t)$), or first order in $\widehat{a}^\dagger\widehat{a}$ will be limited by $\mathrm{var}[\log|f|] \approx \mathrm{var}[\log|\alpha(t)|]$ or $\mathrm{var}[\log|n(t)|]$, respectively.

4.3. Logarithmic variances

The time evolution of the variances of the logarithmic variables can be calculated in the limit $\mathcal{S} \to \infty$ from the formal solutions (16). For the phase-dependent variables it is more convenient to consider just the mean of the variances of the two complementary variables α and β:

$$\mathcal{V} = \tfrac{1}{2}\{\mathrm{var}[\log|\alpha(t)|] + \mathrm{var}[\log|\beta(t)|]\}. \tag{32}$$

Consider coherent-state starting conditions $\widehat{\rho}(0) = \widehat{\Lambda}_0/\mathrm{Tr}[\widehat{\Lambda}_0]$ such that $n(0) = n_0$ for all trajectories. We will use the notation

$$n_0 = n_0' + \mathrm{i}n_0'', \tag{33}$$

etc for real and imaginary parts.

Noting that (1) $\log n$ is exactly Gaussian distributed and (2) in the Ito calculus noises are uncorrelated with any variables at the same or previous times, one obtains from (16)

$$\mathcal{V} = \kappa t/2 + \kappa^2 \int_0^t \mathrm{d}s \int_0^t \mathrm{d}s' \langle n''(s) n''(s') \rangle_{\mathrm{s}}. \tag{34}$$

Now if $s' > s$, then from (16*c*) $\zeta_j(s') = \zeta_j(s) + \widetilde{\zeta}_j(s'-s)$, where $\widetilde{\zeta}_j(t)$ are independent of ζ_j but again with $\langle \widetilde{\zeta}_j(t)\widetilde{\zeta}_k(s)\rangle_{\mathrm{s}} = \delta_{jk}\ \min[t,s]$. It is convenient to define $\zeta^{\pm} = [\zeta_1 \pm \zeta_2]/\sqrt{2}$. Then for $s' > s$

$$\begin{aligned}\langle n''(s)n''(s')\rangle_{\mathrm{s}} &= \mathrm{e}^{-\gamma(s+s')}\langle \mathrm{e}^{-2\sqrt{\kappa}\zeta^-(s)}\rangle_{\mathrm{s}}\langle \mathrm{e}^{-\sqrt{\kappa}\widetilde{\zeta}^-(s'-s)}\rangle_{\mathrm{s}}\langle \cos[\sqrt{\kappa}\widetilde{\zeta}^+(s'-s)]\rangle_{\mathrm{s}} \\ &\quad \times \{(n_0')^2\langle \sin^2[\sqrt{\kappa}\zeta^+(s)]\rangle_{\mathrm{s}} + (n_0'')^2\langle \cos^2[\sqrt{\kappa}\zeta^+(s)]\rangle_{\mathrm{s}} \\ &\quad + n_0' n_0''\langle \sin[2\sqrt{\kappa}\zeta^+(s)]\rangle_{\mathrm{s}}\}. \end{aligned} \tag{35}$$

The trigonometric averages can be evaluated using (25). After some algebra and integration, one obtains

$$\begin{aligned}\lim_{\mathcal{S}\to\infty} \mathcal{V} &= \kappa t/2 - \kappa^2 n_0' \left\{\frac{1-\mathrm{e}^{-\gamma t}(1+\gamma t)}{\gamma^2}\right\} \\ &\quad + \kappa^2|n_0|^2\left\{\frac{1}{q-\gamma}\left[\frac{1-\mathrm{e}^{-\gamma t}}{\gamma} + \frac{\mathrm{e}^{-qt}-1}{q}\right] - \frac{1}{2}\left(\frac{1-\mathrm{e}^{-\gamma t}}{\gamma}\right)^2\right\}, \end{aligned} \tag{36a}$$

where

$$q = 2(\gamma - \kappa) \tag{36b}$$

is a 'damping strength' parameter. Also,

$$\mathrm{var}[\log|n(t)|] = \kappa t. \tag{36c}$$

4.4. Special cases

Two cases are of particular interest: with *no damping* $\gamma = 0$, $\mathcal{V}$ becomes

$$\mathcal{V} = \kappa t/2 - (\kappa t)^2 n_0'/2 + \tfrac{1}{3}(\kappa t)^3|n_0|^2 + \mathrm{O}[(\kappa t)^4|n_0|^2] \tag{37}$$

at low times $2\kappa t \ll 1$, and

$$\mathcal{V} \approx \kappa t/2 + \tfrac{1}{4}|n_0|^2\,\mathrm{e}^{2\kappa t} \tag{38}$$

at $t \gg 1/2\kappa$.

If the damping is small but nonzero ($\gamma t \ll 1$), (37) becomes modified to

$$\mathcal{V} \approx \kappa t/2 - n_0'(\kappa t)^2\big[1 - \tfrac{2}{3}\gamma t\big]/2 + \tfrac{1}{3}|n_0|^2(\kappa t)^3\big[1 - \tfrac{5}{4}\gamma t\big] \tag{39}$$

to order $(\gamma t)^2$ and $(\kappa t)^4$. Also, while $q < 0$, (38) becomes $\mathcal{V} \approx \kappa t/2 + \kappa^2|n_0|^2\,\mathrm{e}^{-qt}/q(q-\gamma)$.

With *strong damping* when $q > 0$, the long-time (i.e. $qt \gg 1$) behaviour becomes asymptotic to a simple linear increase with time

$$\mathcal{V} = \kappa t/2 - b, \tag{40}$$

where

$$b = \frac{\epsilon^2}{2}[2n_0' - |n_0|^2\epsilon/(1-\epsilon)] \tag{41}$$

is a constant and $\epsilon = \kappa/\gamma \in [0,1]$. We note b is positive for strong damping, but later tends towards $-\infty$ as $\epsilon \to 1$. The minimum damping required for positive b grows with mode occupation n_0. The short-time behaviour when $\gamma t \ll 1$ is of the same form as the weakly damped case above.

Referring back to condition (31), we see that while the $n(t)$ distribution remains usable for a relatively long time ($t \lesssim \mathrm{O}(10/\kappa)$) $\approx 1.5 t_{\mathrm{revival}}$, the phase-dependent variables can rapidly acquire very broad distributions (as per (38)) when damping is small and mode occupation is large. This is what limits simulation usefulness.

4.5. Useful simulation time: analytic expressions

While moments containing only the mode occupation $\widehat{n} = \widehat{a}^\dagger \widehat{a}$ can be evaluated for long times of order t_{revival}, this is due to special symmetries present only in the single-mode system. With inter-mode coupling, large spreads in any single $\alpha_{\mathbf{n}}$ will rapidly feed into the remainder of the variables via the coupling terms $\propto \omega_{\mathbf{nm}}$ in equations (11). In particular, evolution of 'occupation' variables $n_{\mathbf{n}}$ is non-trivially coupled to the 'phase' variables $\alpha_{\mathbf{n}}$. With the M-mode systems in mind, then, we are primarily interested in precision of observable estimates in the single-mode model that involves *phase* variables α or β, not just n (e.g. $G^{(1)}$).

Using limits (31) and (36*a*) or its special cases in section 4.4, useful simulation times t_{sim} can be estimated for coherent-state initial conditions (18). For non-coherent-state initial distributions each separate trajectory still starts out as a sample of an off-diagonal coherent-state kernel (18). The useful simulation time is then determined by the shortest useful simulation time to be expected from any of the $\mathcal{S}$ samples.

For *large-mode occupation with no damping* (the worst case), the term in $|n_0|^2(\kappa t)^3$ dominates $\mathcal{V}$ at short times $\kappa t \ll 1$, and

$$t_{\mathrm{sim}} \approx \frac{\mathrm{O}(3)}{\kappa |n_0|^{2/3}}. \tag{42}$$

Checking back, $\kappa t \approx \mathrm{O}(3)/|n_0|^{2/3}$, so (42) is consistent with the short-time assumption for $|n_0| \gg \mathrm{O}(5)$. At weak nonzero damping $\gamma t \ll 1$, (42) becomes modified to

$$t_{\mathrm{sim}} \approx \mathrm{O}(3)/\kappa |n_0|^{2/3}[1 + \mathrm{O}(\gamma/\kappa |n_0|^{2/3})]. \tag{43}$$

At *small occupations* $n_0 \ll 1$, simulation times are longer, and the regime where (38) applies is reached. For a significant range of $|n_0| \ll 1$, the term $\propto |n_0|^2$ dominates $\mathcal{V}$, and the useful simulation time scales very slowly with $|n_0|$ as

$$t_{\mathrm{sim}} \approx \frac{\mathrm{O}(1) - \frac{1}{2}\log|n_0|}{-q/4}. \tag{44}$$

With weak damping, $-q/2 \to \kappa$. At even smaller n_0, the κt term in $\mathcal{V}$ is greater, and

$$t_{\mathrm{sim}} \approx \mathrm{O}(10)/\kappa. \tag{45}$$

For sufficiently *strong damping* such that $q > 0$ and $q t_{\mathrm{sim}} \gg 1$, (40) applies, and long simulation times are possible

$$t_{\mathrm{sim}} \approx \mathrm{O}(b + 10)/\kappa. \tag{46}$$

5. Empirical simulation time results

To verify the analytic estimates, simulations of an undamped single-mode anharmonic oscillator were performed for a wide range of initial coherent states $n_0 = n_0'$ from 10^{-5} to 10^{10}. The primary aim was to determine the actual dependence of useful simulation time t_{sim} on mode occupation, particularly for intermediate n_0 values $\lesssim \mathrm{O}(1)$ where the simple expression (42) does not apply. This is shown in figure 2. These results will be useful for subsequent many-mode simulation time estimates in section 6.

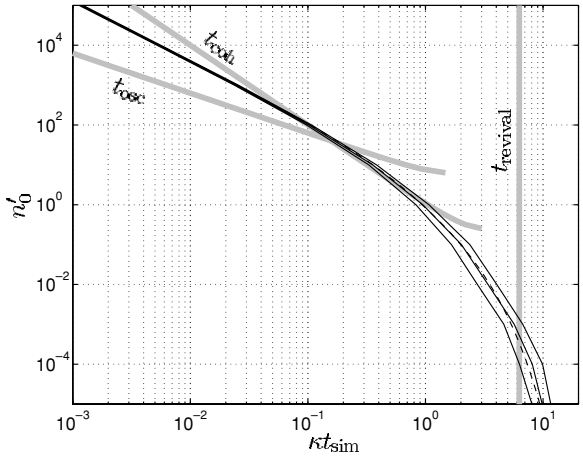

Figure 2. Useful simulation time $t_{\rm sim}$ for a positive P simulation of undamped one-mode system (14) (solid lines). Triple lines indicate observed ranges. Dashed line indicates the best estimate with (48).

Table 2. Empirical fitting parameters for the maximum useful simulation time $t_{\rm sim}$ in one mode. The fit is to expression (48).

c_1	c_2	c_3	c_4
2.54 ± 0.16	$3.2 \pm {}^{\infty}_{1.2}$	-0.5 ± 0.3	0.45 ± 0.07

In what follows, the term *useful precision* for an observable $\widehat{O}$ has been taken to indicate the situation where the estimate $\overline{O} = \langle f \rangle_{\rm s}$ of $\langle \widehat{O} \rangle$ using $\mathcal{S} = 10^6$ trajectories has a relative precision of at least 10% at the one sigma confidence level. This is assuming that the CLT holds so that

$$\Delta \overline{O} \approx \sqrt{\frac{\mathrm{var}[f]}{\mathcal{S}}} \tag{47}$$

is used to assess uncertainty in $\overline{O}$. For the model here, we consider useful precision in the magnitude of phase-dependent correlations $|G^{(1)}(0,t)|$, which is the low-order observable most sensitive to the numerical instabilities in the equations.

Uncertainties in the calculated $t_{\rm sim}$ times arise because $\Delta|G^{(1)}|$ were themselves estimated from finite ensembles of $\mathcal{S} = 10^4$ trajectories. The range of $t_{\rm sim}$ indicated in figure 2 was obtained from ten independent runs with identical parameters.

Taking the analytic scalings (42) and (44) at high and low n_0 into account, parameters in an approximate curve

$$t_{\rm est} = \frac{1}{\kappa}\left\{[c_1 (n_0')^{-2/3}]^{-c_2} + \left[2\log\left(\frac{\mathrm{e}^{c_3}}{{n_0'}^{c_4}} + 1\right)\right]^{-c_2}\right\}^{-1/c_2} \tag{48}$$

have been fitted to the empirical data. Best values of c_j are given in table 2, and in figure 2 this fit is compared to the empirical data, and seen to be quite accurate. c_1 characterizes the pre-factor for high n_0', c_3 is a constant residual $t_{\rm sim}$ at near vacuum, c_4 characterizes the curvature at small n_0', while c_2 is related to the stiffness of the transition. Expression (48) reduces to $c_1 {n_0'}^{-2/3}/\kappa$ and $(c_3 - c_4 \log n_0')/(\kappa/2)$, when $n_0' \gg 1$ and $n_0' \ll 1$, respectively.

Uncertainty Δc_j in parameters c_j was worked out by requiring $\sum_{n_0}\{[t_{\rm est}(c_j \pm \Delta c_j, n_0) - t_{\rm sim}(n_0)]/\Delta t_{\rm sim}\}^2 = \sum_{n_0}\{1 + ([t_{\rm est}(c_j, n_0) - t_{\rm sim}(n_0)]/\Delta t_{\rm sim})^2\}$.

6. Multi-mode simulation times

6.1. Extrapolation to many modes

First, let us note that for each mode **n** the nonlinearity that leads to rapid growth of distribution broadness at $\mathcal{V} \approx 10$ depends only on the local variables $\alpha_{\mathbf{n}}$ and $\beta_{\mathbf{n}}$. This suggests that extrapolating the single-mode results of the previous section may lead to usable simulation time estimates for the coupled M-mode system.

If the distribution of an amplitude variable in any mode acquires broad and/or rapidly growing tails (e.g. due to the single-mode instability caused by the nonlinearity), the coupling terms $\propto \omega_{\mathbf{nm}}$ rapidly disseminate its influence to the remaining modes, and all observables acquire large uncertainty. This effectively terminates the useful part of the simulation. From (42) and/or figure 2, we can see that for a single weakly damped mode $t_{\rm sim}$ drops off rapidly with increasing mode occupation n_0. At the same time the distributions of its phase variables broaden rapidly, and this broadness is distributed into the rest of the modes. Thus, the most highly occupied mode of a many-mode system limits the overall simulation time.

6.2. Simulation time estimate

If we assume (for the time being) that inter-mode coupling does not significantly affect the time in which the most highly occupied mode reaches $\mathcal{V} \approx 10$, one estimates that

$$t_{\rm sim} \approx t_{\rm est}\left(\max_{(t \lesssim t_{\rm est}, \mathbf{n})}[\overline{n}_{\mathbf{n}}(t)]\right), \tag{49}$$

where $\overline{n}_{\mathbf{n}}(t)$ is the mean occupation $\langle \widehat{a}^\dagger_{\mathbf{n}} \widehat{a}_{\mathbf{n}} \rangle$ at time t, and $t_{\rm est}$ is given by (48). Using the mean value $\overline{n}$ appears justified since for usefully precise simulations at higher occupations we expect $|n(t) - \overline{n}(t)| \ll \overline{n}(t)$. For strongly damped systems, (46) applies rather than $t_{\rm est}$.

For a model arising as the discretization of a continuum-field model (1) with density $\rho(\mathbf{x})$, $\overline{n}_{\mathbf{n}} \approx \rho(\mathbf{x}_{\mathbf{n}})\Delta V$. When $\max(\overline{n}_{\mathbf{n}}(t)) \gg 1$, the estimated simulation time becomes

$$t_{\rm sim} \approx \left(\frac{2.5\hbar}{g}\right) \frac{(\Delta V)^{1/3}}{\left(\max_{(t \lesssim t_{\rm est}, \mathbf{x})}[\rho(\mathbf{x})]\right)^{2/3}}. \tag{50}$$

What was perhaps not obvious before obtaining the above expression is that *coarser lattices lead to longer simulations*. The useful time scales as $(\Delta V)^{1/3}$ in the strong interaction limit. Thus, when simulating a field model, it is worthwhile to use the coarsest lattice for which physical predictions are not affected.

6.3. Influence of kinetics in the multi-mode case

Linear coupling between modes is what complicates the physical behaviour, and consequently also the noise behaviour in a simulation. Let us use the label $z_{\mathbf{n}}$ for either $\alpha_{\mathbf{n}}$ or $\beta_{\mathbf{n}}$, and look at the short-time fluctuations of the phase-space variables. These fluctuations can be separated as

$$\delta z_{\mathbf{n}}(t) \approx \delta^{\rm direct} z_{\mathbf{n}}(t) + \delta^{\rm kinetic} z_{\mathbf{n}}(t), \tag{51}$$

into the 'direct' part due to local inter-particle scattering as considered in detail for the single-mode anharmonic oscillator (14), and secondary 'kinetic' fluctuations. These are mostly due

to transfer of direct fluctuations between modes by the kinetic inter-mode coupling, at least initially.

If $\delta^{\text{direct}} z_{\mathbf{n}}(t) \gg \delta^{\text{kinetic}} z_{\mathbf{n}}(t)$, then properties based on the single-mode analysis (such as the simulation time estimates (49) and (50)) will be qualitatively accurate. A rough calculation for uniform gases at density ρ (see the appendix for details) shows that at short times,

$$\frac{\text{var}[|\delta^{\text{kinetic}} z_{\mathbf{n}}(t)|]}{\text{var}[|\delta^{\text{direct}} z_{\mathbf{n}}(t)|]} \approx \text{O}\left[\frac{\hbar^2 t^2 \pi^4}{60 m^2 (\Delta V)^{4/D}}\right], \tag{52}$$

while the right-hand side is $\ll 1$. This is independent of the uniform density itself, and indicates that the additional fluctuations due to kinetic effects

(i) become relatively more important with time and
(ii) are more dominant for fine lattices.

Once (52) becomes $\gtrsim \text{O}(1)$, deviations from the simulation time estimates of section 6.2 can be expected, although this simple analysis does not tell us whether inter-mode coupling decreases or increases simulation time. In general a decrease seems intuitively more likely, but an increase may occur if $\delta^{\text{direct}} z_{\mathbf{n}}(t)$ and $\delta^{\text{kinetic}} z_{\mathbf{n}}(t)$ become appropriately correlated to reduce overall fluctuations.

7. Multi-mode example: 1D gas

7.1. Model

As an example of many-mode dynamical simulations, we have simulated a uniform one-dimensional gas of bosons with density ρ and inter-particle s-wave scattering length a_s. The lattice is chosen with a spacing $\Delta x_d \gg a_s$ so that inter-particle interactions are effectively local at each lattice point, and the lattice Hamiltonian (2) applies. The stochastic equations to simulate are (11). Periodic boundary conditions are assumed.

The initial state is taken to be a $T = 0$ coherent wavefunction, which is a stationary state of the ideal gas (i.e. when $a_s = g = 0$). Subsequent evolution is with constant $a_s > 0$, so that there is a disturbance at $t = 0$ when inter-particle interactions are rapidly turned on.

Physically, this would correspond to the disturbance created in a BEC by rapidly increasing the scattering length at $t \approx 0$ by tuning the external magnetic field near a Feshbach resonance. Behaviour found in this uniform system will carry over without qualitative change to a 1D BEC confined on a length significantly larger than the length scale of observed dynamical phenomena. Most of these phenomena extend over the order of a healing length

$$\xi^{\text{heal}} = \frac{\hbar}{\sqrt{2m\rho g}}. \tag{53}$$

This is the minimum length scale over which a local density inhomogeneity in a Bose condensate wavefunction can be in balance with the quantum pressure due to kinetic effects [19].

A useful time scale here is

$$t_\xi = \frac{m(\xi^{\text{heal}})^2}{\hbar} = \frac{\hbar}{2\rho g} \tag{54}$$

(the 'healing time'), which is approximately the time needed for the short-distance $\text{O}(\xi^{\text{heal}})$ inter-atomic correlations to equilibrate after the disturbance [8].

7.2. Spatial correlations

Here we calculate the dynamics of spatial correlation functions, which has not been previously investigated from first principles in this model. We consider values averaged over the location of one particle out of the pair/triplet since this is a uniform gas.

First order:

$$\overline{g}^{(1)}(\mathbf{x_n}) = \frac{1}{M}\sum_{\mathbf{m}} \frac{\langle \widehat{a}^\dagger_{\mathbf{m}} \widehat{a}_{\mathbf{m+n}}\rangle}{\sqrt{\langle \widehat{a}^\dagger_{\mathbf{m}} \widehat{a}_{\mathbf{m}}\rangle \langle \widehat{a}^\dagger_{\mathbf{m+n}} \widehat{a}_{\mathbf{m+n}}\rangle}}. \tag{55}$$

This is a phase-dependent correlation function. Its magnitude $|\overline{g}^{(1)}|$ tells one the degree of first-order spatial coherence, while its phase gives the relative phase of the wavefunction at distances $\mathbf{x_n}$.

Second order:

$$\overline{g}^{(2)}(\mathbf{x_n}) = \frac{1}{M}\sum_{\mathbf{m}} \frac{\langle \widehat{a}^\dagger_{\mathbf{m}} \widehat{a}^\dagger_{\mathbf{m+n}} \widehat{a}_{\mathbf{m}} \widehat{a}_{\mathbf{m+n}}\rangle}{\langle \widehat{a}^\dagger_{\mathbf{m}} \widehat{a}_{\mathbf{m}}\rangle \langle \widehat{a}^\dagger_{\mathbf{m+n}} \widehat{a}_{\mathbf{m+n}}\rangle}. \tag{56}$$

This describes the likelihood of finding two particles at a distance $\mathbf{x_n}$ from each other, relative to what is expected of a coherent field. For a bunched field, $\overline{g}^{(2)}(\mathbf{x}) > 1$ (e.g. a thermal state has $\overline{g}^{(2)}(\mathbf{x}) = 2$), while spatial antibunching is evidenced by $\overline{g}^{(2)}(\mathbf{x}) < 1$.

Third order:

$$\overline{g}^{(3)}(\mathbf{x_n}) = \frac{1}{M}\sum_{\mathbf{m}} \frac{\langle \widehat{a}^\dagger_{\mathbf{m}} \widehat{a}^\dagger_{\mathbf{m+n}} \widehat{a}^\dagger_{\mathbf{m-n}} \widehat{a}_{\mathbf{m}} \widehat{a}_{\mathbf{m+n}} \widehat{a}_{\mathbf{m-n}}\rangle}{\langle \widehat{a}^\dagger_{\mathbf{m}} \widehat{a}_{\mathbf{m}}\rangle \langle \widehat{a}^\dagger_{\mathbf{m+n}} \widehat{a}_{\mathbf{m+n}}\rangle \langle \widehat{a}^\dagger_{\mathbf{m-n}} \widehat{a}_{\mathbf{m-n}}\rangle}. \tag{57}$$

This three-particle correlation function describes the likelihood of three particles with (equal) distances $\mathbf{x_n}$ between nearest neighbours (relative to a coherent field). In a BEC, the rate of three-body recombination, which can limit the condensate's lifetime, is proportional to $\overline{g}^{(3)}(0)$ [20].

7.3. Comparison with simulation time estimates

A number of positive P simulations of a one-dimensional gas were made, with densities of $\rho = 100/\xi^{\mathrm{heal}}$, $10/\xi^{\mathrm{heal}}$ and $1/\xi^{\mathrm{heal}}$, and various lattice spacings. The number of lattice points was varied between simulations taking on values from $M = 25$ to $M = 500$ depending on circumstances to encompass and resolve the phenomena seen. More lattice points were required at the higher densities where correlations were weaker, resulting in longer simulation times overall.

Figure 3 compares the actual useful simulation times in simulations with what was predicted by expressions (49) and (50). We can see that the fit is remarkably good despite inter-mode coupling. It is also clearly seen that the simulation time decreases with $\Delta x = \overline{n}/\rho$.

Note that values of t_{sim} are based on precision in $\overline{g}^{(2)}$. Precision tends to become worse as higher-order moments of $\widehat{a}$ or $\widehat{a}^\dagger$ become needed, in e.g. $\overline{g}^{(3)}$. This is simply because higher-order moments require the averaged quantity f to be a higher-order polynomial in α and β, and in effect $\mathrm{var}[\log|f|] \approx c^2\mathcal{V}$, with c being approximately the order of moment.

Figures 4–7 show calculated correlation functions for the example system $\rho = 1/\xi^{\mathrm{heal}}$. We see enhanced pairing/tripling of particles at several preferred relative distances. These preferred inter-particle distances increase with time. Note that the local density $\rho(\mathbf{x}, t)$ is completely invariant, and *this wave-like behaviour is seen only in the correlations*. It is interesting to note that the overall disturbance advances at a much faster rate than the

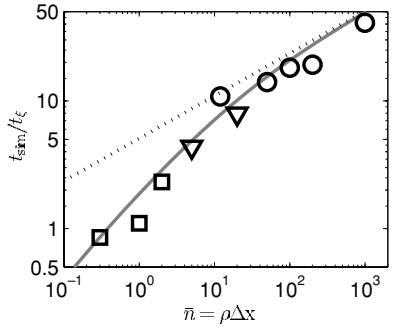

Figure 3. Comparison of the useful simulation time $t_{\rm sim}$ to the estimates (50) (dotted) and (49) (grey line). $t_{\rm sim}$ based on precision in $\overline{g}^{(2)}(x)$. Data points for simulations of 1D gases of densities $100/\xi^{\rm heal}$, $10/\xi^{\rm heal}$ and $1/\xi^{\rm heal}$ are shown with circles, triangles and squares, respectively. $\mathcal{S} = 10^4$ trajectories.

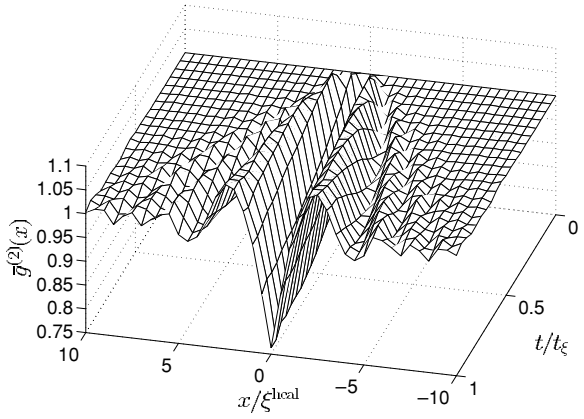

Figure 4. Second-order correlations in a uniform 1D gas with density $\rho = 1/\xi^{\rm heal}$. 50 lattice points, $\Delta x = \xi^{\rm heal}/2$, and $\mathcal{S} = 10^4$ trajectories.

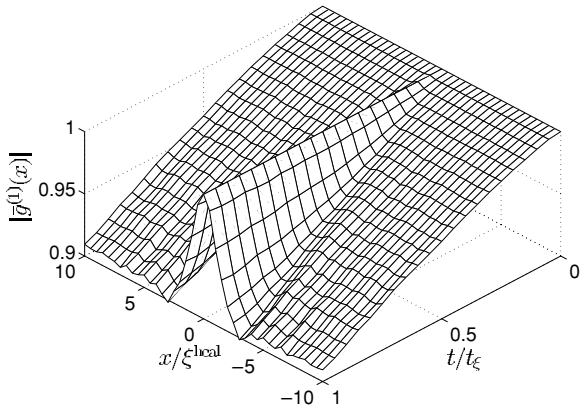

Figure 5. First-order correlations. Details as in figure 4.

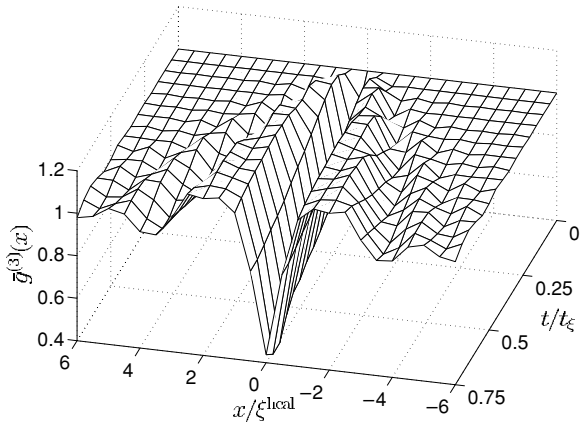

Figure 6. Third-order correlations. Details as in figure 4.

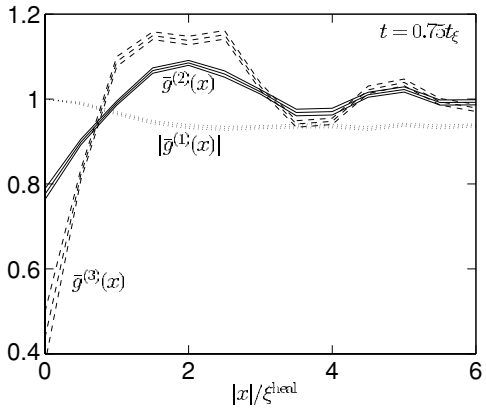

Figure 7. Correlations at $t = 0.75t_\xi$. Triple lines indicate error bars at one σ. Details as in figure 4.

peaks/troughs of the correlations. We also see that while long-range coherence is steadily lost, there is a short-distance scale corresponding to the distance of the nearest two-particle correlation peak on which phase coherence is enhanced compared to the long-range situation.

Significantly more details regarding calculations with the uniform gas and the correlation waves seen can be found in [8], chapter 10.

8. Conclusions

We have obtained the following.

- Simulation time estimates (49) and (50) for many-mode positive P simulations, the former using the fitting curve (48) and empirical data of table 2, the latter applicable at maximum mode occupation $\gg 1$. It was found that useful simulation time decreases with density and increases with lattice spacing (coarseness).
- These simulation time estimates were found to be accurate for simulations of uniform 1D gases.

- Dynamics of spatial correlation behaviour (first to third order) in an interacting uniform 1D gas after disturbance due to change in scattering length. Propagating 'correlation waves' in second- and third-order correlations (figures 4 to 7) were seen.
- Detailed characterization of the behaviour of a single spatial mode (14) in an interacting Bose gas model.
- Estimates (52) of relative importance of direct and coupling-induced fluctuations in phase variables at short times.

A comparison with other more recently proposed methods was made in table 1, and it is seen that each has its own merits, depending on the model. In broad terms the advantages of the positive P/gauge P method are its simplicity and versatility. Equations to simulate are just the GP mean-field equations with added Gaussian noise which, remarkably, is sufficient to account for all quantum mechanical features. Also, there is no truncation of entanglement, no hard-wired conservation laws, and open systems are the standard. The method is trivially adaptable to parallel computation; just run each trajectory separately.

The dynamical timescales that can be simulated in a given system using the positive P method, can be easily assessed 'on the back of an envelope' using the simulation time estimates given here.

Appendix. Scattering and kinetic fluctuations

The aim here is to assess the relative strength of fluctuations in phase-dependent variables due to direct noise terms $\propto\sqrt{\kappa}$ and to mixing of noise ($\propto\omega_{\mathbf{nm}}$) from other modes by kinetic processes. A uniform gas of density ρ, with $\gamma = V_{\rm ext} = 0$, is considered, and we use the notation of section 6.3. We denote the linear coupling terms in equations (11) as

$$\begin{aligned} \mathrm{d}z_{\mathbf{n}} &= -\mathrm{i}\sum_{\mathbf{m}} \omega_{\mathbf{nm}} z_{\mathbf{m}}\,\mathrm{d}t + \cdots \\ &= -\mathrm{i}\mathcal{E}^{(z)}_{\mathbf{n}}\,\mathrm{d}t + \cdots, \end{aligned} \tag{A.1}$$

where z can denote either the variable α or β^*. Kinetic terms in the Hamiltonian (1) lead to

$$\mathcal{E}^{(z)}_{\mathbf{n}} = \frac{\hbar}{2mM}\sum_{\mathbf{m},\widetilde{\mathbf{n}}} z_{\mathbf{m}}|\mathbf{k}_{\widetilde{\mathbf{n}}}|^2\,\mathrm{e}^{\mathrm{i}\mathbf{k}_{\widetilde{\mathbf{n}}}\cdot(\mathbf{x}_{\mathbf{n}}-\mathbf{x}_{\mathbf{m}})}, \tag{A.2}$$

on a lattice with M points. $\widetilde{\mathbf{n}} = (\widetilde{n}_1,\ldots,\widetilde{n}_D)$ labels lattice points in a Fourier space such that $\mathbf{k}_{\widetilde{\mathbf{n}}} = (\Delta k_1\widetilde{n}_1,\ldots,\Delta \mathrm{k}_D\widetilde{N}_D)$, where $\Delta k_d = 2\pi/L_d$, and L_d is the full lattice extent in the d dimension.

Since the gas is uniform, mean conditions at each lattice point must be identical, and random variables can be written as the sum of a global mean part and local fluctuations:

$$\mathcal{E}^{(z)}_{\mathbf{n}}(t) = \overline{\mathcal{E}}^{(z)}(t) + \delta\mathcal{E}^{(z)}_{\mathbf{n}}(t), \qquad z_{\mathbf{n}}(t) = \overline{z}(t) + \delta z_{\mathbf{n}}(t). \tag{A.3}$$

Due to lack of external forces $|\overline{z}(t)| = \sqrt{\rho\Delta V}$.

Let us denote the $z_{\mathbf{n}}$ fluctuations when no inter-mode coupling is present (i.e. $\mathcal{E}^{(z)}_{\mathbf{n}} = 0$) as $\delta^{\rm direct}z_{\mathbf{n}}$. In this case the formal solutions (16) apply to each mode independently. At *short times* $\kappa t \ll 1$ the nonlinear drift term initially acts mainly as a deterministic time-varying phase, and so the dominant fluctuating contribution would be due directly to the noise terms. Then

$$\log\alpha_{\mathbf{n}}(t) \approx \log\overline{\alpha}(t) + \mathrm{i}\sqrt{\mathrm{i}\kappa}\,\zeta_{1\mathbf{n}}(t), \qquad \log\beta_{\mathbf{n}}(t) \approx \log\overline{\beta}(t) + \sqrt{\mathrm{i}\kappa}\,\zeta_{2\mathbf{n}}(t). \tag{A.4}$$

with $\zeta_{j\mathbf{n}}$ being random variables of the (16*c*) kind and independent for each $\mathbf{n}$. At short enough times that $\mathrm{var}[\log|z_{\mathbf{n}}(t)|] \ll 1$, one then has

$$\begin{aligned} z_{\mathbf{n}}(t) &\approx \overline{z}(t) + \overline{z}(t)[\log z_{\mathbf{n}}(t) - \log \overline{z}(t)] \\ &= \overline{z}(t) + \delta^{\mathrm{direct}} z_{\mathbf{n}}(t). \end{aligned} \tag{A.5}$$

Using (A.4), (A.5) and properties (17), one finds

$$\mathrm{var}[|\delta^{\mathrm{direct}} z_{\mathbf{n}}(t)|] \approx \frac{\rho g t}{\hbar}. \tag{A.6}$$

Now for the kinetic-induced fluctuations. At short times while these are small, i.e. $\mathrm{var}[|\delta^{\mathrm{kinetic}}|] \ll \mathrm{var}[|\delta^{\mathrm{direct}}|]$, the additional fluctuations in the local terms due to the mode-mixing can be ignored, and so the remaining fluctuations due to coupling are just $\delta^{\mathrm{kinetic}} z_{\mathbf{n}}(t) \approx -\mathrm{i}\int_0^t \delta\mathcal{E}_{\mathbf{n}}^{(z)}(s)\,\mathrm{d}s$. Using (A.2), and substituting in for $z_{\mathbf{m}}$ with the approximate (direct noise only) short-time expression $z_{\mathbf{m}} \approx \overline{z} + \delta^{\mathrm{direct}} z_{\mathbf{m}}$, one obtains

$$\begin{aligned} \mathrm{var}[|\delta^{\mathrm{kinetic}} z_{\mathbf{n}}(t)|] \approx{}& \left(\frac{\hbar}{2mM}\right)^2 \int_0^t \mathrm{d}t' \int_0^t \mathrm{d}t'' \\ &\times \sum_{\mathbf{m},\mathbf{m}',\tilde{\mathbf{n}},\tilde{\mathbf{n}}'} \langle \delta^{\mathrm{direct}} z^*_{\mathbf{m}'}(t'') \delta^{\mathrm{direct}} z_{\mathbf{m}}(t')\rangle_{\mathrm{s}} |\mathbf{k}_{\tilde{\mathbf{n}}}|^2 |\mathbf{k}_{\tilde{\mathbf{n}}'}|^2 \, \mathrm{e}^{-\mathrm{i}\mathbf{k}_{\tilde{\mathbf{n}}'}\cdot(\mathbf{x}_{\mathbf{n}}-\mathbf{x}_{\mathbf{m}'})} \, \mathrm{e}^{\mathrm{i}\mathbf{k}_{\tilde{\mathbf{n}}}\cdot(\mathbf{x}_{\mathbf{n}}-\mathbf{x}_{\mathbf{m}})}. \end{aligned} \tag{A.7}$$

Since the direct noise at each lattice point in the locally interacting model is independent, then $\langle \delta^{\mathrm{direct}} z^*_{\mathbf{m}'}(t'') \delta^{\mathrm{direct}} z_{\mathbf{m}}(t')\rangle_{\mathrm{s}} = \delta_{\mathbf{m},\mathbf{m}'}\rho g \ \min[t'', t']/\hbar$, similar to (A.6). After performing the integrations over t' and t'' and simplifying the Fourier transforms one obtains

$$\mathrm{var}[|\delta^{\mathrm{kinetic}} z_{\mathbf{n}}(t)|] \approx \mathrm{var}[|\delta^{\mathrm{direct}} z_{\mathbf{n}}(t)|] \frac{\hbar^2 t^2}{12m^2 M} \sum_{\tilde{\mathbf{n}}} |\mathbf{k}_{\tilde{\mathbf{n}}}|^4. \tag{A.8}$$

For a D-dimensional system with many modes, one can approximate

$$\sum_{\tilde{\mathbf{n}}} |\mathbf{k}_{\tilde{\mathbf{n}}}|^4 \approx \frac{M\Delta V}{(2\pi)^D} \int |\mathbf{k}|^4 d^D\mathbf{k} = \frac{c_1(\mathbf{k}^{\max}) M \pi^4}{5(\Delta V)^{4/D}}, \tag{A.9}$$

where $c_1(\mathbf{k}^{\max})$ is a shape factor O(1) that depends on the ratios between momentum cutoffs $k_d^{\max} = \pi/\Delta \mathrm{x}_d$ in the various lattice dimensions. For example, in 1D, $c_1 = 1$, while for 2D and 3D when the momentum cutoffs in each dimension are equal, one has $c_1 = 3\frac{1}{9}$, and $c_1 = 6\frac{1}{3}$. Substituting into (A.8) one obtains the final estimate (52).

References

[1] Chaturvedi S, Drummond P D and Walls D F 1977 *J. Phys. A: Math. Gen.* **10** L187–92
[2] Drummond P D and Gardiner C W 1980 *J. Phys. A: Math. Gen.* **13** 2353
[3] Drummond P D and Deuar P 2003 *J. Opt. B: Quantum Semiclass. Opt.* **5** S281
[4] Cetinbas M and Wilkie J 2004 *Preprint* quant-ph/0407036
[5] Deuar P and Drummond P D 2005 *Preprint* cond-mat/0501058 (*J. Phys. A: Math. Gen.* submitted) (see also [8])
[6] A treatment of these issues can be found in Leggett A J 2001 *Rev. Mod. Phys.* **73** 307
For a more detailed treatment see Weiner J, Bagnato V S, Zilio S and Julienne P S 1999 *Rev. Mod. Phys.* **71** 1
[7] Deuar P and Drummond P D 2002 *Phys. Rev.* A **66** 033812
[8] See also Deuar P 2004 *PhD Thesis* The University of Queensland (*Preprint* cond-mat/0507023) in preparation
[9] See e.g. Gardiner C W 1991 *Quantum Noise* (Berlin, Heidelberg: Springer)
Gardiner C W 1983 *Handbook of Stochastic Methods* (Berlin, New York: Springer)
[10] Carter S J, Drummond P D, Reid M D and Shelby R M 1987 *Phys. Rev. Lett.* **58** 1841
Drummond P D, Shelby R M, Friberg S R and Yamamoto Y 1993 *Nature* **365** 307
[11] Drummond P D and Corney J F 1999 *Phys. Rev.* A **60** R2661
[12] Steel M J, Olsen M K, Plimak L I, Drummond P D, Tan S M, Collett M J, Walls D F and Graham R 1998 *Phys. Rev.* A **58** 4824

[13] Drummond P D, Deuar P and Kheruntsyan K V 2004 *Phys. Rev. Lett.* **92** 040405
[14] Carusotto I, Castin Y and Dalibard J 2001 *Phys. Rev.* A **63** 023606
[15] Castin Y and Carusotto I 2001 *J. Phys. B: At. Mol. Opt. Phys.* **34** 4589
[16] Vidal G 2003 *Phys. Rev. Lett.* **91** 147902
Vidal G 2004 *Phys. Rev. Lett.* **93** 040502
Zwolak M and Vidal G 2004 *Phys. Rev. Lett.* **93** 207205
[17] Verstraete F, Garcia-Ripoll J J and Cirac J I 2004 *Phys. Rev. Lett.* **93** 207204
Verstraete F and Cirac J I 2004 *Preprint* cond-mat/0407066
[18] Vidal G, Latorre J I, Rico E and Kitaev A 2003 *Phys. Rev. Lett.* **90** 227902
[19] See e.g. Dalfovo F, Giorgini S, Pitaevskii L P and Stringari S 1999 *Rev. Mod. Phys.* **71** 463 481
[20] Kagan Yu, Svistunov B V and Shlyapnikov G V 1988 *JETP Lett.* **48** 56